PAPER

Probing the origin of lateral heterogeneities in synthetic monolayer molybdenum disulfide

2D Materials

PAPER

Probing the origin of lateral heterogeneities in synthetic monolayer molybdenum disulfide

RECEIVED
23 October 2018

REVISED
17 December 2018

ACCEPTED FOR PUBLICATION
7 January 2019

PUBLISHED
1 February 2019

Kehao Zhang[1,2], Yuanxi Wang[3], Jaydeep Joshi[4,5], Fu Zhang[1], Shruti Subramanian[1], Mauricio Terrones[1,3,6], Patrick Vora[4,5], Vincent Crespi[1,3,6] and Joshua A Robinson[1,2,7]

[1] Department of Materials Science and Engineering and Center for Two Dimensional and Layered Materials, The Pennsylvania State University, University Park, PA 16802, United States of America
[2] Center for Atomically Thin Multifunctional Coatings, The Pennsylvania State University, University Park, PA 16802, United States of America
[3] 2-Dimensional Crystal Consortium & Materials Research Institute, The Pennsylvania State University, University Park, PA 16802, United States of America
[4] Department of Physics and Astronomy, George Mason University, Fairfax, VA 22030, United States of America
[5] Quantum Materials Center, George Mason University, Fairfax, VA 22030, United States of America
[6] Department of Chemistry, The Pennsylvania State University, University Park, PA 16802, United States of America
[7] Author to whom any correspondence should be addressed.

E-mail: jrobinson@psu.edu

Keywords: 2D Materials, molybdenum disulfide, heterogeneities

Supplementary material for this article is available online

Abstract

Synthetic two-dimensional (2D) materials provide an opportunity to realize large-scale applications in next generation electronic and optoelectronic devices. One of the biggest challenges of synthetic 2D materials is the lateral heterogeneity such as non-uniform strain, composition and defect density. The electronic and optical properties are found to be not uniform in many cases, even within a single crystalline domain, potentially limiting synthetic 2D materials in advanced devices. In this work, we probe the origin of the widely observed lateral heterogeneities in synthetic monolayer MoS_2. Epitaxial single crystalline domains (~10 μm) are optically homogeneous and uniform with 0.3%–0.4% tensile strain, while misoriented domains (>20 μm) exhibit distinct photoluminescence (PL) emissions from the center to the edge, along with released strain at the center. Temperature-dependent Raman and PL mapping reveals that the center of non-epitaxial domains exhibits an enhanced PL due to increased defect density. Density function theory (DFT) calculations suggest that oxygen defects can readily lead the loss of epitaxy, consistent with our observation of a MoO_x core–shell structure that only exists in misoriented domains. Combining experiment and DFT, we hypothesize that two growth mechanisms, solid–solid and vapor–solid growth, may be responsible for the lateral heterogeneities.

Introduction

Exploration and expansion of 2D materials property libraries [1–4] and applications demonstrates their potential to be relevant in next-generation electronic, optoelectronic, sensing and energy harvesting applications [4, 5]. Recently, large scale synthesis of 2D materials brings these materials one step closer to industrially compatible applications [6–8]. However, the current quality of synthetic materials cannot meet the requirements for investigations in spintronics [9], topological devices [10] and quantum physics [11, 12] due to high defect density and orders of magnitude defect density variation based on different growth methods (~10^{12} cm^{-2} for high purity MOCVD grown WSe_2 [6] and 10^{13}–10^{14} cm^{-2} for powder based CVD grown MoS_2 [13], and 10^{11}–10^{12} cm^{-2} for mechanically exfoliated MoS_2 [14]). Defect populations in a single-crystal flake are often spatially non-uniform and are closely related to uncontrolled modulation of parameters during growth, leaving a crystal with heterogeneous response to external probes [15].

Heterogeneity in synthetic 2D films is typically probed by optical measurements such as photoluminescence (PL) mapping and second harmonic

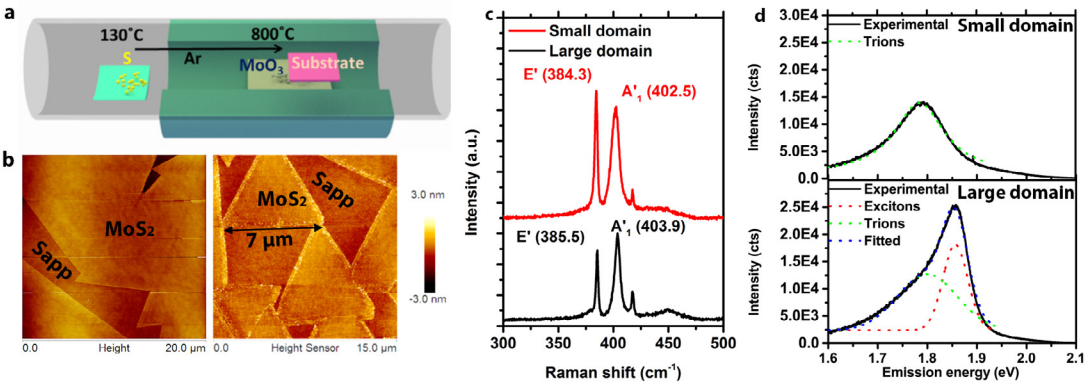

Figure 1. Domain size dependent heterogeneity in synthetic monolayer MoS_2. (a) Schematic of the growth of monolayer MoS_2; (b) AFM images of L-MoS_2 (left) and S-MoS_2 (right), indicating no secondary layer on monolayer MoS_2; (c) Raman spectra extracted from point scan at the center of L-MoS_2 (black) and S-MoS_2 (red), variations in A_1 and E' peak suggests higher electron concentration and tensile strain in S-MoS_2; (d) PL spectra comparison between L-MoS_2 (bottom) and S-MoS_2 (top). Trions emission is dominating in S-MoS_2, while both excitons and trions emission are observed in L-MoS_2.

generation (SHG) [15–19]. Depending on the local defect density and misorientation [17], or strain [15], the PL intensity of monolayer MoS_2 can be reduced or enhanced. This is exemplified in the work by Bao and Borys *et al* [20], who utilize a near-field nanoprobe to visualize the local heterogeneity and identify two distinct optoelectronic regions with subwavelength resolution (<60 nm) in synthetic monolayer MoS_2 on SiO_2. The edge region of a single crystalline domain is energetically disordered with hybrid emission from excitons and trions, due to higher sulfur vacancies along the edge of the MoS_2 domain. Recent studies demonstrate that oxygen defects, particularly Mo–O bonding, is able to enhance the PL by tens of times and significantly increase the carrier life time [16, 17]. Furthermore, Carozo *et al* combines low temperature PL and high-resolution scanning transmission electron microscopy (HRSTEM) to identify the highly sulfur deficient WS_2 edge regions can introduce defect-bound excitons visible at low temperature (77 K), marked as the first unambiguous assignment of defect-related PL to a specific type in 2D TMDs [21].

Heterogeneity depends on substrate choice. This is evident when comparing as-grown monolayer WS_2 single crystalline domains to transferred domains to a new SiO_2 substrate, where a 50 meV shift of ground state exciton and ~0.25% reduction of tensile strain is identified [22], indicating the film-substrate coupling during the growth may play an important role in the heterogeneity. Indeed, the film-substrate interaction is stronger than the ideal van der Waals interaction, especially in epitaxy [6, 17]. To date, most heterogeneity studies on synthetic 2D materials are on SiO_2 [15, 20, 22], with few on 'epi-ready' substrates such as sapphire [6]. As epitaxy is one of the most important techniques to achieve the industrially compatible 2D materials, it is critical to understand the origin of heterogeneities resulting from epitaxial growth.

In this work, we demonstrate that the origin of lateral heterogeneity in epitaxial monolayer MoS_2 on sapphire is oxygen rich defects in single crystalline domains. Small domains (S-MoS_2 hereafter, ~10 μm) exhibit aligned crystal orientation, and uniform PL emission and strain, while large domains (L-MoS_2 hereafter, >20 μm) lose orientation alignment and exhibit a sharp lateral transition under optical probes. Doubled PL intensity and 0.3%−0.4% released tensile strain is observed in the center region (~15 μm) of L-MoS_2. Counterintuitively, this region correlates to a highly defective region, as characterized by PL mapping of defect emission at low temperature (5 K). The observation of a MoO_x core shell structure in the center of L-MoS_2 along with density functional theory (DFT) calculations suggest that the O defect may be responsible for the loss of epitaxy and lateral heterogeneities. Moreover, based on all the experimental and computational results, we propose two distinct growth mechanisms respectively dominating the earlier growth of L-MoS_2 and the later growth of S-MoS_2, explaining their difference in defect such as MoO_x density and orientation uniformity. L-MoS_2 nucleates earlier and is grown under a solid–solid mechanism, where MoO_x is condensed on the substrate and subsequently sulfurized, resulting in an O-defective center region. S-MoS_2 nucleates later, after which both S-MoS_2 and the edge region of L-MoS_2 are grown under a vapor–solid mechanism, where MoS_2 is formed in vapor-phase and condensed onto the substrate.

Results and discussion

Domain size is a key indicator of epitaxial MoS_2 orientation, strain, and electron concentration heterogeneities. Monolayer MoS_2 on sapphire is synthesized by powder vaporization (figure 1(a)), in which 2 mg MoO_3 and 200 mg S powder is heated to 800 °C and 130 °C respectively, with 100 sccm Ar as the carrier gas (figures 1(a) and Figure S1a (stacks.iop.org/TDM/6/025008/mmedia)) [17, 23]. Optical microscopy (OM) images (figures S1(b) and (c)) show

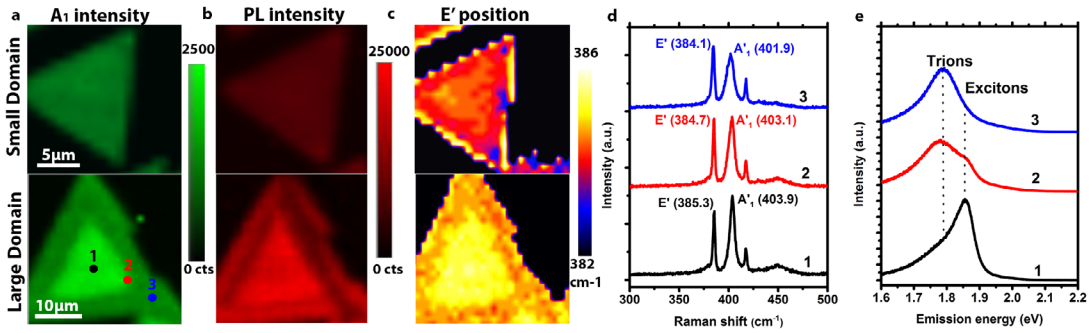

Figure 2. Local heterogeneity of MoS_2 monolayer. (a) and (b) A_1 intensity, PL intensity and E' intensity map of S-MoS_2 (top row) and L-MoS_2 (bottom row). The results show that the strain and optical properties of S-MoS_2 are more uniform in the single crystalline domain, while the center region of L-MoS_2 exhibits higher electron concentration and lower strain; (d) and (e) representative PL and Raman spectra extracted from 1 to 3 labeled in figure (a).

that growth includes aligned S-MoS_2 and randomly oriented L-MoS_2. Figure 1(b) is an atomic force microscopy (AFM) image of L-MoS_2 (left) and S-MoS_2 (right), both are monolayer in thickness without particles/3D islands. Raman and PL measurements performed at the center of each type of domains show that the A_1 peak of S-MoS_2 is 1.4 cm^{-1} red shifted, broadened and quenched compared to L-MoS_2, indicating higher electron concentration in S-MoS_2 [24]. E' peak of S-MoS_2 is 1.2 cm^{-1} blue shifted. Applying the strain/E' shift ratio: 3.2–4 cm^{-1}/% in literature [25–27], the S-MoS_2 exhibits 0.3%–0.4% tensile strain. PL spectra comparison between L-MoS_2 and S-MoS_2 shows further distinction. The PL spectra of S-MoS_2 are dominated by trions emission with negligible excitons emission, while L-MoS_2 shows exciton emission and trion emission with similar spectral weights. The energy difference between the exciton peak and trion peak is 58 meV, indicating the high electron concentration in the MoS_2 film in both cases, agreeing with Raman measurements (figures 1(c) and (d)) [28]. The relatively higher trions bounding energy can be due to the higher electron concentration [17, 28].

Heterogeneity is characterized by a sharp transition in the L-MoS_2 single crystalline domain. Figures 2(a)–(c) presents the A_1 intensity, PL intensity and E' position maps of S- and L-MoS_2 as the indicator of electron concentration, PL emission and strain, respectively. The electron concentration, PL emission and strain is consistently more uniform in S-MoS_2 than L-MoS_2. The center of L-MoS_2 exhibits lower electron concentration, higher PL emission and lower tensile strain compared to the edge. Local properties are compared by averaging a 3 × 3 pixel region (2.25 μm^2) from the PL and Raman map from three locations [1–3] noted in figure 2(a) of the L-MoS_2. Quenching of exciton emission from the center to the edge reveals an increased electron concentration (figure 2(d)) [28]. Representative Raman spectra further confirms the trend of electron concentration as A_1 peak is redshifted, quenched and broadened (figure 2(e)) [24]. Red shift of E' peak from the center to the edge suggests higher tensile strain along the edge of MoS_2 [26]. The lateral PL variations (peak intensity, peak position from the center to the edge of the domain) are substantial regardless the laser power. Power-dependent PL shows the increased photo-induced trions as the power increase (figure S2) [29]. However, the photo-induced trions emission is negligible compared to the change from the center to the edge of the domain. Trions emission always dominates the emission at the edge while excitons emission contributes most at the center under all characterized laser powers (figure S3). Interestingly, the local, lateral changes of PL and Raman characteristics are sudden instead of gradual, indicating that the origin of the heterogeneity cannot only be attributed to the depletion of MoO_3.

Raman and PL heterogeneities spatially correlate with heterogeneous defect concentrations, evident by low temperature PL. Low-temperature PL measurements are carried out at 5 K using 532 nm (2.33 eV) laser excitation to probe the effects of domain sizes and associated growth mechanisms on excitonic emission [21, 30]. Spectra from all domains required the subtraction of the background PL from the sapphire substrate (figure S5). The grown flakes typically range in size from 10 μm to 50 μm, with an A-exciton emission at 1.88 eV [15]. As the temperature is reduced, a low-energy defect emission at 1.7 eV begins to dominate the PL spectra, especially as the domain size increases. The size-dependent low temperature PL spectra (figure 3(a)), clearly shows that the defect emission peak increases as the domain size increase, suggesting that higher defect concentration exists as the domain grows larger. Spatial PL intensity map integrated in the range of 1.6 eV–1.8 eV (defect emission region) further provides the insights of the lateral distribution of defects density (figures 3(b) and (c)). While the ~10 μm domains exhibit a low intensity defect emission relative to exciton recombination process (figure 3(b)), defect emission dominates the PL spectra at the center of large flakes (~30 μm) (figure 3(c)). The lateral defect density comparison (figures S6(a) and (b)) suggests that the defect density, particularly sulfur vacancies at the center of a large triangular domain is ~2× higher

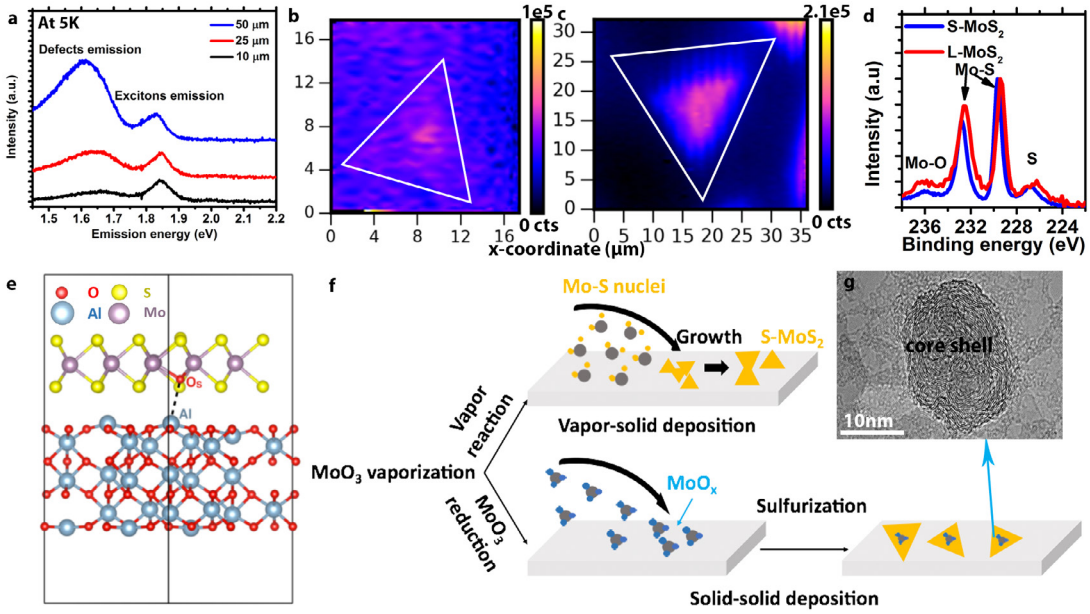

Figure 3. Defect and growth mechanism of PV grown MoS_2. (a) Size-dependent PL spectra from the center of MoS_2 domains taken at 5 K. The defect emission increases with the domain size; (b) and (c) 5 K spatial PL map of S-MoS_2 and L-MoS_2 in defect emission range, respectively. The defect emission is negligible in S-MoS_2, while the defect emission is concentrated at the center platelet of L-MoS_2; (d) XPS comparison in Mo 3d region between L-MoS_2 and S-MoS_2, suggesting 12% higher Mo–O concentration in L-MoS_2. (e) An oxygen substitution of sulfur O_S pins to a surface Al atom by 0.1 eV; (f) Hypothesized growth mechanisms of PV grown MoS_2, which can be responsible for the lateral heterogeneities; (g) HRTEM image of the centerplate of L-MoS_2, a clear core–shell structure is observed.

than the edge of a large domains and small domains. Interestingly, the contour of the defect-concentrated center region of L-MoS_2 matches well with the shape of PL-enhanced domain centers in L-MoS_2 (figure 2(b)). Prior works [16, 17] demonstrate that oxygen rich defects (i.e. O at sulfur vacancies [14]), can be responsible for the defect-enhanced PL of MoS_2. Indeed, x-ray photoelectron spectroscopy (XPS) measurements confirms a 12% higher Mo–O concentration in the L-MoS_2 region. Figure 3(d) shows the XPS comparison between Mo 3d spectra acquired in the L-MoS_2 region (red curve) and S-MoS_2 region (blue curve). Beyond the significant Mo–S bonding at 229.6 eV and 232.7 eV, Mo–O boding at 235.5 eV is clearly visualized in both cases. Mo–O bonding in L-MoS_2 exhibits clearly higher intensity than S-MoS_2 [17, 31]. Detailed peak fitting and analysis (figure S7) suggests ~23% Mo intensity comes from Mo–O in L-MoS_2, while 11% Mo intensity is from Mo–O in S-MoS_2, confirming the O defect is responsible for the PL enhancement in this study. Note that the noisier XPS spectra from L-MoS_2 is attributed to the lower coverage of MoS_2 (figures S1(b) and (c)). Attempts are made to identify the defect type via high resolution scanning transmission electron microscopy (HRSTEM). However, we are not able to distinguish the contrast between 2-O and 1-S due to their equal Z number.

Density functional theory (DFT) calculations indicate that oxygen defects can lead to a loss of epitaxy. The orientation locking of MoS_2 on sapphire at 0/60° is a robust registry effect, since stacking at these preferred angles are energetically more favorable than intermediate angles by 100 meV/MoS_2 unit (estimated as an upper bound by previous DFT calculations) [32], compared to the weaker 2 meV orientational preference per MoS_2 unit for stacking on hBN. The strong orientation selectivity is related to the overall strong adhesion between the exposed surface of Al atoms on the sapphire surface and the bottom layer sulfur in MoS_2 (with attractive electrostatic interactions in addition to vdW), as quantified by their ~30 meV $Å^{-2}$ adhesion energy from DFT calculations [33], stronger than the typical 20 meV $Å^{-2}$ interlayer adhesion between the conventional vdW heterostacks [34]. Interruption of this strong orientation selectivity requires two ingredients: an initial mis-registration during nucleation, and that it remains incorrect during subsequent growth due to defect pinning. To investigate possible substrate pinning, we employ DFT to calculate the interaction between a sapphire substrate and a simple, innocuous oxygen defect in the MoS_2—an isolated oxygen substitution of sulfur O_S (figure 3(e)). Compared with the average adhesion between a sapphire surface and a MoS_2 monolayer including one O_S (averaged over multiple interlayer translational offsets in the lateral direction, each structurally relaxed), the adhesion when O_S is near a surface Al atoms is stronger by 0.1 eV (per O_S), so that O_S–Al affinity can be characterized by the same strength. Given sufficient concentration, multiple defects pinning at surface Al atoms can overpower the orientation selectivity demanded by lattice commensuration. The use of O_S only serves as a conservative example that a simple defect like one isolated oxygen substitution of sulfur can easily

disable substrate epitaxy, in reality more complex oxygen defects are expected since a simple O_S would not yield the defect emission observed in low temperature PL, likely with even stronger substrate pinning potentials. In the current work, we find a MoO_x core–shell structure only at the center of L-MoS_2 using high-resolution transmission electron microscope (HRTEM) (figure 3(g)), suggesting that the initial nucleation seeds of L-MoS_2 are MoO_x or O-rich MoS_2 (solid–solid growth) [35]. Further HRSTEM image and corelated energy dispersive spectroscopy (EDS) map confirms the high oxygen concentration at the core–shell (figure S8). In the oxide-based PV growth of MoS_2, many intermediate products such as $(MoO_3)_3$ clusters, reduced MoO_{3-x} and MoO_2 can form near the substrate surface [35]. Products with lower melting point such as $(MoO_3)_3$ clusters ($T_m = 795$ °C), maintain high vapor pressure and can react with sulfur vapor to form MoS_2 in vapor phase, while other products with higher melting point such as MoO_2 ($T_m = 1100$ °C), is condensed on the substrate, followed by sulfurization. If it is not rapidly sulfurized to persist in vapor phase, MoO_2 clusters have to condense on the substrate as the nuclei due to the higher melting point of MoO_2. Since the crystal structure of MoO_2 (distorted rutile) is different from sapphire (hexagonal), the sapphire substrate is not able to guide the orientation of MoO_2, leading to loss of epitaxy. We have thus shown that in both limits—the O-rich limit where the nucleation seed is MoO_x (as identified by HRTEM) and the O-poor limit where domains contain dilute amounts of oxygen point defects (as conservatively estimated from DFT calculations)—epitaxy is destroyed.

The measured release of tensile strain (figures 1(c) and 2(c)) in L-MoS_2 is a direct consequence of its loss of epitaxy. The $< 1\%$ tensile strain in epitaxial MoS_2 (S-MoS_2) on sapphire is likely due to the small deviation from a 3:2 lattice commensuration ($a_{MoS_2} = 3.15$ Å [36], $a_{sapp} = 4.76$ Å [37], lattice mismatch $= 1 - \frac{3.15\times3}{4.76\times2} \approx 1\%$). Epitaxial S-$MoS_2$ nucleates later than L-MoS_2 and is grown under the vapor–solid mechanism (figure 3(f)), where MoS_2 is formed before condensation on the substrate. Therefore, S-MoS_2 has sufficiently large crystalline areas and low oxygen-defects to allow epitaxy on the substrate due to their shared hexagonal crystal structure, 3:2 commensurability and orientation-dependent stacking energies [32, 38] between MoS_2 and sapphire. In contrast, L-MoS_2 nucleates with MoO_x clusters in the early stage and is grown under the solid–solid mechanism Interestingly, the optical and defect properties along the edge of the L-MoS_2 is similar to the epitaxial S-MoS_2, which is attributed to the edge guided vapor-solid deposition [39], providing another evidence that epitaxial S-MoS_2 nucleates later than L-MoS_2.

In summary, we report the lateral size dependent heterogeneity of PV grown monolayer MoS_2 on sapphire. PL and Raman characterizations suggest strong film/substrate interaction (strain) when the single crystalline domain is epitaxial, featuring small and oriented domains, while the tensile strain is relaxed at the center platelet of MoS_2 single crystals when epitaxy fails, featuring large and misoriented domains. Low-T PL measurements reveal that the relaxed interaction is closely related to the concentrated defects, agreeing with 12% higher Mo–O concentration identified by XPS. Evident by DFT calculations, the defects, specifically O defects, are responsible for the failure of epitaxy. All the evidence indicates two distinct growth mechanisms: vapor–solid epitaxy and solid–solid sulfurization may be the origin of the heterogeneities.

Acknowledgment

KZ, SS and JAR acknowledges the Center for Atomically Thin Multifunctional Coatings (ATOMIC), sponsored by the National Science Foundation (NSF) division of Industrial, Innovation & Partnership (IIP) under award #1540018. SS and JAR acknowledge the funding from NSF CAREER (Award: 1453924). YW and VC acknowledge the National Science Foundation Materials Innovation Platform Two-Dimensional Crystal Consortium under DMR-1539916 and XSEDE (TG-DMR170050) for allocation on LSU superMIC cluster. MT acknowledges The Air Force Office of Scientific Research (AFOSR) grant 17RT0244. FZ and MT were partially supported by the Basic Office of Science of the Department of Energy under award DE-SC0018025. PMV and JJ acknowledge support from the National Science Foundation under Grant No. 1748650 and from the GMU Quantum Materials Center.

ORCID iDs

Kehao Zhang https://orcid.org/0000-0003-4405-2438
Yuanxi Wang https://orcid.org/0000-0002-0659-1134
Fu Zhang https://orcid.org/0000-0003-1841-5880
Shruti Subramanian https://orcid.org/0000-0002-8933-9486
Patrick Vora https://orcid.org/0000-0003-3967-8137
Vincent Crespi https://orcid.org/0000-0003-3846-3193

References

[1] Zhou J *et al* 2018 A library of atomically thin metal chalcogenides *Nature* **556** 355–9
[2] Lin Z *et al* 2016 2D materials advances: from large scale synthesis and controlled heterostructures to improved characterization techniques, defects and applications *2D Mater.* **3** 042001
[3] Bhimanapati G R *et al* 2015 Recent advances in two-dimensional materials beyond graphene *ACS Nano* **9** 11509–39
[4] Stanford M G, Rack P D and Jariwala D 2018 Emerging nanofabrication and quantum confinement techniques for 2D materials beyond graphene *npj 2D Mater. Appl.* **2** 20

[5] Jariwala D, Sangwan V K, Lauhon L J, Marks T J and Hersam M C 2014 Emerging device applications for semiconducting two-dimensional transition metal dichalcogenides *ACS Nano* **8** 1102–20
[6] Lin Y-C *et al* 2018 Realizing large-scale, electronic-grade two-dimensional semiconductors *ACS Nano* **12** 965–75
[7] Kang K, Xie S, Huang L, Han Y, Huang P Y, Mak K F, Kim C-J, Muller D and Park J 2015 High-mobility three-atom-thick semiconducting films with wafer-scale homogeneity *Nature* **520** 656–60
[8] Zhang K *et al* 2018 Large scale 2D/3D hybrids based on gallium nitride and transition metal dichalcogenides *Nanoscale* **10** 336–41
[9] Pesin D and MacDonald A H 2012 Spintronics and pseudospintronics in graphene and topological insulators *Nat. Mater.* **11** 409–16
[10] Li J, Wang K, McFaul K J, Zern Z, Ren Y, Watanabe K, Taniguchi T, Qiao Z and Zhu J 2016 Gate-controlled topological conducting channels in bilayer graphene *Nat. Nanotechnol.* **11** 1060
[11] Scuri G *et al* 2018 Large excitonic reflectivity of monolayer $MoSe_2$ encapsulated in hexagonal boron nitride *Phys. Rev. Lett.* **120** 037402
[12] Wang K *et al* 2018 Electrical control of charged carriers and excitons in atomically thin materials *Nat. Nanotechnol.* **13** 128–32
[13] Hong J *et al* 2015 Exploring atomic defects in molybdenum disulphide monolayers *Nat. Commun.* **6** 6293
[14] Pető J, Ollár T, Vancsó P, Popov Z I, Magda G Z, Dobrik G, Hwang C, Sorokin P B and Tapasztó L 2018 Spontaneous doping of the basal plane of MoS_2 single layers through oxygen substitution under ambient conditions *Nat. Chem.* **10** 1246
[15] Liu Z *et al* 2014 Strain and structure heterogeneity in MoS_2 atomic layers grown by chemical vapour deposition *Nat. Commun.* **5** 5246
[16] Nan H *et al* 2014 Strong photoluminescence enhancement of MoS_2 through defect engineering and oxygen bonding *ACS Nano* **8** 5738–45
[17] Zhang K *et al*2017 Deconvoluting the photonic and electronic response of 2D materials: the case of MoS_2 *Sci. Rep.* **7** 16938
[18] Yin X, Ye Z, Chenet D A, Ye Y, O'Brien K, Hone J C and Zhang X 2014 Edge nonlinear optics on a MoS_2 atomic monolayer *Science* **344** 488–90
[19] Cheng J, Jiang T, Ji Q, Zhang Y, Li Z, Shan Y, Zhang Y, Gong X, Liu W and Wu S 2015 Kinetic nature of grain boundary formation in As-grown MoS_2 monolayers *Adv. Mater.* **27** 4069–74
[20] Bao W *et al* 2015 Visualizing nanoscale excitonic relaxation properties of disordered edges and grain boundaries in monolayer molybdenum disulfide *Nat. Commun.* **6** 1–7
[21] Carozo V*et al* 2017 Optical identification of sulfur vacancies: Bound excitons at the edges of monolayer tungsten disulfide *Sci. Adv.* **3** e1602813
[22] McCreary K M, Hanbicki A T, Singh S, Kawakami R K, Jernigan G G, Ishigami M, Ng A, Brintlinger T H, Stroud R M and Jonker B T 2016 The effect of preparation conditions on Raman and photoluminescence of monolayer WS_2 *Sci. Rep.* **6** 35154
[23] Ruzmetov D *et al* 2016 Vertical 2D/3D semiconductor heterostructures based on epitaxial molybdenum disulfide and gallium nitride *ACS Nano* **10** 3580–8
[24] Chakraborty B, Bera A, Muthu D V S, Bhowmick S, Waghmare U V and Sood A K 2012 Symmetry-dependent phonon renormalization in monolayer MoS_2 transistor *Phys. Rev.* B **85** 161403(R)
[25] Zhu C R *et al* 2013 Strain tuning of optical emission energy and polarization in monolayer and bilayer MoS2 *Phys. Rev.* B **88** 121301
[26] Conley H J, Wang B, Ziegler J I, Haglund R F, Pantelides S T and Bolotin K I 2013 Bandgap engineering of strained monolayer and bilayer MoS_2 *Nano Lett.* **13** 3626–30
[27] Lee J-U, Woo S, Park J, Park H C, Son Y-W and Cheong H 2017 Strain-shear coupling in bilayer MoS_2 *Nat. Commun.* **8** 1370
[28] Mak K F, He K, Lee C, Lee G H, Hone J, Heinz T F and Shan J 2012 Tightly bound trions in monolayer MoS_2 *Nat. Mater.* **12** 207–11
[29] Wang X H, Ning J Q, Su Z C, Zheng C C, Zhu B R, Xie L, Wu H S and Xu S J 2016 Photoinduced doping and photoluminescence signature in an exfoliated WS_2 monolayer semiconductor *RSC Adv.* **6** 27677–81
[30] Tongay S *et al* 2013 Defects activated photoluminescence in two-dimensional semiconductors: interplay between bound, charged, and free excitons *Sci. Rep.* **3** 2657
[31] Addou R *et al* 2015 Impurities and electronic property variations of natural MoS_2 crystal surfaces *ACS Nano* **9** 9124–33
[32] Dumcenco D *et al* 2015 Large-area epitaxial monolayer MoS_2 *ACS Nano* **9** 4611–20
[33] Singh A K, Hennig R G, Davydov A V and Tavazza F 2015 Al_2O_3 as a suitable substrate and a dielectric layer for *n*-layer MoS_2 *Appl. Phys. Lett.* **107** 053106
[34] Björkman T, Gulans A, Krasheninnikov A V and Nieminen R M 2012 van der Waals bonding in layered compounds from advanced density-functional first-principles calculations *Phys. Rev. Lett.* **108** 235502
[35] Zak A, Feldman Y, Alperovich V, Rosentsveig R and Tenne R 2000 Growth mechanism of MoS_2 fullerene-like nanoparticles by the gas phase synthesis *J. Am. Chem. Soc.* **122** 11108–16
[36] Young P A 1968 Lattice parameter measurements on molybdenum disulphide *J. Phys. D: Appl. Phys.* **1** 936–8
[37] Yim W M and Paff R J 1974 Thermal expansion of AlN, sapphire, and silicon *J. Appl. Phys.* **45** 1456–7
[38] Ji Q, Kan M, Zhang Y, Guo Y, Ma D, Shi J, Sun Q, Chen Q, Zhang Y and Liu Z 2015 Unravelling orientation distribution and merging behavior of monolayer MoS_2 domains on sapphire *Nano Lett.* **15** 198–205
[39] Chen L, Liu B, Ge M, Ma Y, Abbas A N and Zhou C 2015 Step-edge-guided nucleation and growth of aligned WSe_2 on sapphire via a layer-over-layer growth mode *ACS Nano* **9** 8368–75